International Journal of Innovative
Computing, Information and Control
Volume **14**, Number **6**, December **2018**

 ISSN 1349-4198
pp. **2203–2219**

MODELING AND QUANTITATIVE DESIGN OF A CONTROLLER FOR A BIDIRECTIONAL CONVERTER WITH HIGH VOLTAGE CONVERSION RATIO

Pi-Yun Chen, Kuei-Hsiang Chao and Hong-Jhih Chen

Department of Electrical Engineering
National Chin-Yi University of Technology
No. 57, Sec. 2, Zhongshan Rd., Taiping Dist., Taichung 41170, Taiwan
{ chenby; chaokh }@ncut.edu.tw; free_0207@hotmail.com

Received January 2018; revised July 2018

Abstract. *The purpose of this paper is to perform the quantitative design of high voltage conversion ratio bidirectional converter controller applied in photovoltaic power generation system. In order to keep the voltage dynamic response of load step change with the features of zero steady-state error, no overshoot, small voltage-drop and fast restore time, we perform the quantitative design of a controller by the given performance specification. First, we use the step response estimation method at the selected operation point to estimate the dynamic model of the converter. Then, we follow the given load regulation performance to make the quantitative design of controller's parameters, enable the converter's output DC link voltage be controlled at the planned dynamic and steady-state response performance with stable energy supply. Finally, we use the measured results to verify the performance of the designed controller.*

Keywords: Photovoltaic power generation system, High voltage conversion ratio bidirectional converter, Quantitative design, Step response estimation method, Load regulation

1. **Introduction.** Nowadays the global awakening of boosting power-saving to protect environment, which drives the massive applications of power generation by renewable energy, and the photovoltaic power generation is the largest share of them. The photovoltaic system uses either the boost or buck converter to convert power, yet if converter connects to the photovoltaic module array directly without any control, it cannot fully utilize the photovoltaic module array to generate power. Thus, using the maximum power point tracker (MPPT) to sustain the photovoltaic module array with maximum power output at varied irradiance and temperatures is an important studying subject. Output of the maximum power point tracker normally is connected to the bidirectional step up/down converter to get the bidirectional power flow in DC link. In normal, to perform the goal of storing power by battery and assist the power-supply, it will simultaneously connect the low-voltage side to a battery set and the high-voltage side to the DC voltage bus. Figure 1 shows the proposed system frame [1]. However, to sustain the power quality of DC bus, it needs to use the controller design of bidirectional converter to make the photovoltaic module array maintain the voltage set by the DC bus under different powers generated at varied irradiance and temperatures, controls the voltage steady-state error and overshoot caused by the variation of irradiance to be zero by means of the controller, and makes the voltage drop small and restore time short. Although the existing bidirectional converter framework has high-voltage-up/down ability, normally it uses the try-and-error method

DOI: 10.24507/ijicic.14.06.2203

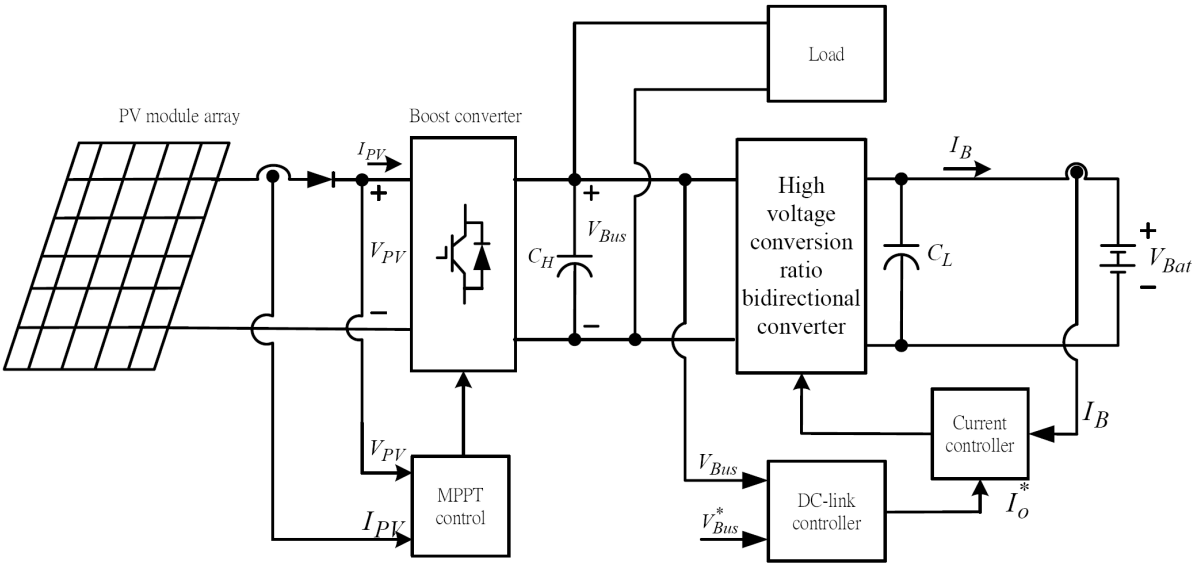

FIGURE 1. System frame used in high voltage conversion ratio bidirectional converter of photovoltaic power generation system

to decide the proportional-integral (PI) controller parameters [2-6], which will make system voltage unstable, or even unable to get the planned DC bus voltage. The voltage controller designed by using Bode plots of frequency response [7,8] can find the voltage controller parameters at the specific operation point, yet if the operation point shifts, it is unable to get a better load regulation performance. At present we already have the intelligent controller such as the fuzzy controller [9,10], sliding-mode controller [11-13] and model predictive control [14], which can get better control performance, yet the controller design is complicated, and with the stability and hard-to-implement issues. Some robust and optimal controllers are presented in [15-18], but they still have the problem of complex computation and implementation. Some of the controllers mentioned above are not robust, and even if they are robust, they are not easy to implement because of the complexity of computing. Therefore, to get better robustness and easy for implementation, the quantitative performance design method is proposed for the proposed high voltage conversion ratio bidirectional converter controller in this paper.

Based on this, in this paper, we use the step response estimation method to estimate the dynamic model of converter. Then, follow the given load regulation performance specifications to perform the quantitative design of controller parameters, which controls the DC link voltage of converter output at the planned dynamic and steady-state performance without any unstable issue. In dealing with the current-controlled PWM scheme, the small-signal mode of current loop is first found using the state-space averaging method, and then, the current controller parameters are found based on frequency response. After deriving the dynamic model of the proposed converter, a systematic design technique has been adopted to find the parameters of a PI voltage controller according to the prescribed specifications. The effectiveness of the proposed controller will be confirmed by simulation and experimental results. Therefore, this controller can be systematized for quantitative design and meets the required performance specifications.

In this paper, Section 2 describes briefly the operating theory of the proposed bidirectional high voltage converter ratio converter. Then, the modeling and quantitative design of a controller for the proposed converter are made in Section 3. In Section 4, some simulation and experimental results are made to demonstrate the effectiveness of the proposed controller. Finally, in Section 5, some conclusions are given.

2. **Operating Theory of Bidirectional High Voltage Conversion Ratio Converter.** The high voltage conversion ratio bidirectional converter mentioned in this paper has the high step-up voltage and high step-down voltage function and bidirectional flow of energy; it connects the high-voltage side to the DC link and low-voltage side to a battery set to perform the battery-power-storage and assist-to-supply-power [4]. The high voltage conversion ratio bidirectional converter circuit applied in this paper is shown in Figure 2. This DC-DC converter with coupled inductors has a simple configuration and an easy-to-use feature, provides an improved voltage gain by use of coupled inductors, and suppresses the input and output ripple current. The operating principle of the proposed bidirectional high voltage conversion ratio converter will be explained more clearly below.

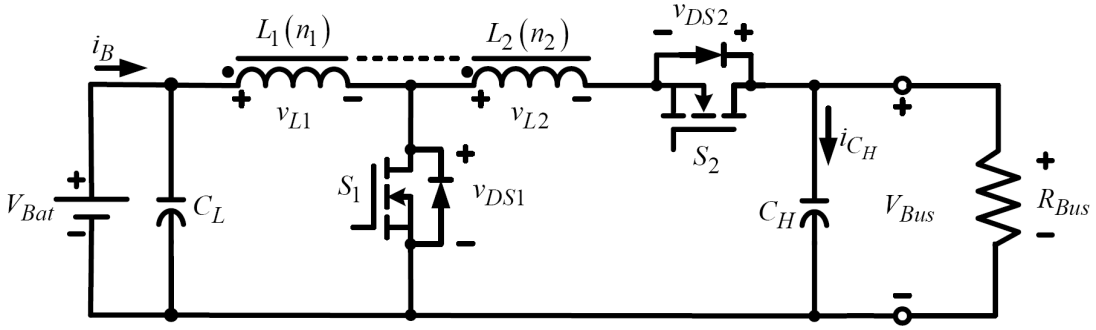

FIGURE 2. The high voltage conversion ratio bidirectional converter circuit

Since the circuit of high voltage conversion ratio bidirectional converter has two-way-flow ability, following the flow direction the energy can be divided into the boost and buck operation modes; the circuit operations can be divided into the closed and open circuit according to the switch actions. In an operating period, the ratio of closed time t_{on}, the ratio of opened time t_{off} and period T within an operating period is defined as the duty ratio D, expressed in Equation (1).

$$D \triangleq \frac{t_{on}}{T} = \frac{t_{on}}{t_{on} + t_{off}} \tag{1}$$

In the following section, we will illustrate the operation theory of high voltage conversion ratio bidirectional converter by the boost mode and buck mode.

2.1. **Boost mode.**

(1) Switch-closed ($0 \leqq t_{on} \leqq D_1 T$)

When the switch S_1 at low-voltage side is closed, since the switch-control signals at both the high voltage (HV) and low voltage (LV) side apply the complementary control method, S_2 at HV side is at off state; the responded equivalent circuit of the converter is shown in Figure 3; now, the voltages measured at both ends of inductors L_1 and L_2 can be expressed as

$$v_{L1} = V_{Bat} = L_1 \frac{di_{L1}}{dt} \tag{2}$$

$$v_{L2} = V_{Bat} \frac{n_2}{n_1} \tag{3}$$

where V_{Bat} is the voltage at low voltage side; n_1 and n_2 are turns of the coupled inductor in primary and secondary sides, respectively.

If the turns ratio of coupled inductor N is defined as

$$N \triangleq \frac{n_2}{n_1} \tag{4}$$

associating Equation (3) we get

$$v_{L2} = NV_{Bat} \tag{5}$$

$$v_L = v_{L1} + v_{L2} = (1+N)V_{Bat} \tag{6}$$

(2) Switch-open ($D_1T \leqq t_{off} \leqq T$)

When S_1 at LV side is opened and S_2 at HV side is closed, the responded equivalent circuit of the converter is shown in Figure 4; now, the coupled inductors L_1 and L_2 can be treated as one inductor L, voltage across L is expressed as

$$v_L = V_{Bat} - V_{Bus} \tag{7}$$

From the volt-second balance theorem of inductor, while operating at steady-state, change of inductor's circuit within a period should be zero; therefore, from Equations (6) and (7) we get

$$(1+N)V_{Bat}D_1T + (V_{Bat} - V_{Bus})(1-D_1)T = 0 \tag{8}$$

After associating Equation (8) we can derive the relation equation of voltages at LV and HV sides as

$$\frac{V_{Bus}}{V_{Bat}} = \frac{(1+ND_1)}{(1-D_1)} \tag{9}$$

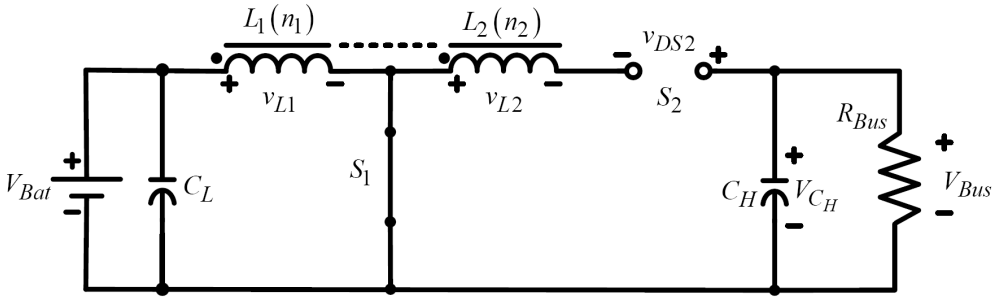

FIGURE 3. Equivalent circuit when S_1 at LV side is closed while the high voltage conversion ratio bidirectional converter is at boost mode

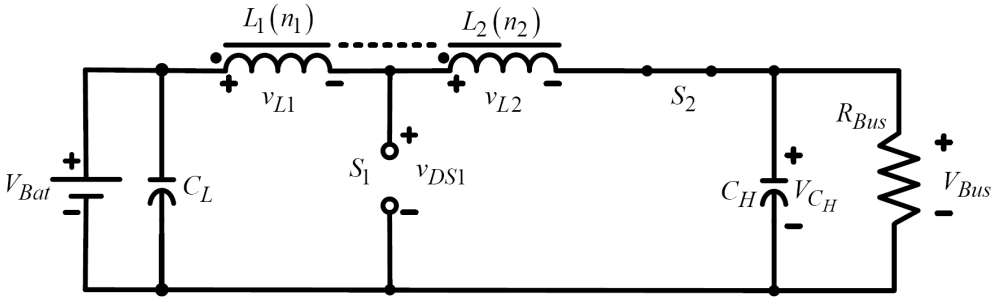

FIGURE 4. Equivalent circuit when S_1 at LV side is opened while the high voltage conversion ratio bidirectional converter is at boost mode

2.2. **Buck mode.**

(1) Switch-closed ($0 \leqq t_{on} \leqq D_2T$)

When switch S_2 at HV side is closed, since the switch-control signals at both the HV and LV sides apply the complementary control method, S_1 at LV side is at off state; the responded equivalent circuit of the converter is shown in Figure 5; now, the coupled inductors L_1 and L_2 can be treated as one inductor L, and voltage across L is expressed as

$$v_L = v_{L1} + v_{L2} = V_{Bat} - V_{Bus} \tag{10}$$

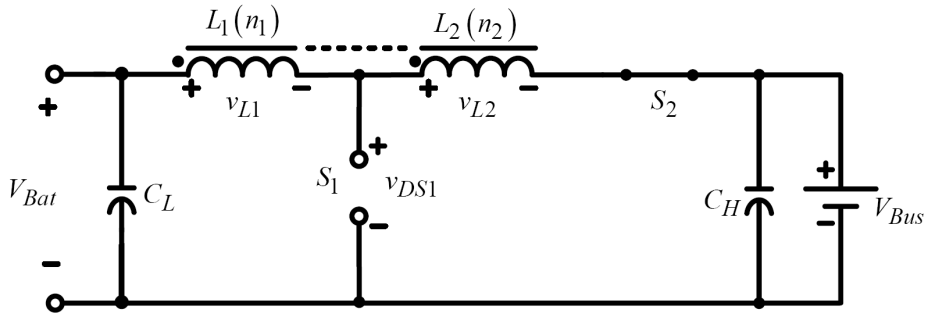

FIGURE 5. Equivalent circuit when S_2 at HV side is closed while the high voltage conversion ratio bidirectional converter is operated at buck mode

(2) Switch-open ($D_2T \leqq t_{off} \leqq T$)

When the switch S_2 at HV side is opened and S_1 at LV side is closed, the responded equivalent circuit of the converter is shown in Figure 6; now, the voltages measured across inductors L_1 and L_2 can be expressed as

$$v_{L1} = V_{Bat} = L_1 \frac{di_{L1}}{dt} \tag{11}$$

$$v_{L2} = V_{Bat} \frac{n_2}{n_1} = NV_{Bat} \tag{12}$$

$$v_L = v_{L1} + v_{L2} = (1 + N)V_{Bat} \tag{13}$$

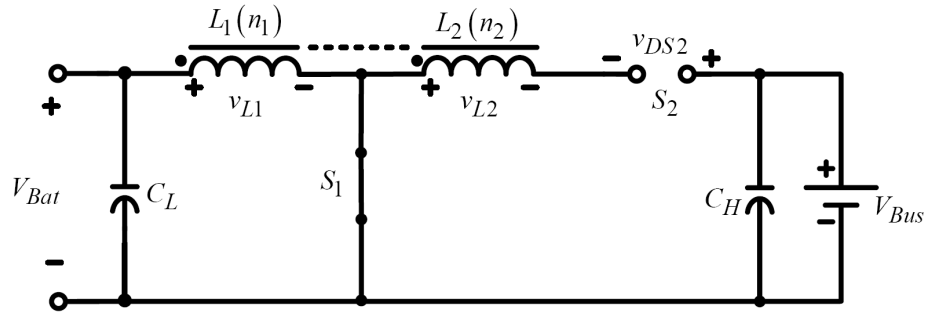

FIGURE 6. Equivalent circuit when S_2 at HV side is opened while the high voltage conversion ratio bidirectional converter is operated at buck mode

From the volt-second balance theorem of inductor, while operating at steady-state, change of inductor's circuit within a period should be zero; therefore, from Equations (10) and (13) we get

$$(V_{Bat} - V_{Bus})D_2T + (1 + N)V_{Bat}(1 - D_2)T = 0 \tag{14}$$

After associating Equation (14) we can derive the relation equation of voltages at LV and HV sides as

$$\frac{V_{Bat}}{V_{Bus}} = \frac{D_2}{1 + N(1 - D_2)} \tag{15}$$

Since the switch-control signals at both the HV and LV sides apply the complementary control method, if D_2 is the duty ratio of switch S_2, then, D_1, the duty ratio of switch S_1, can be expressed as

$$D_1 \triangleq (1 - D_2) \tag{16}$$

Substituting Equation (16) into (15), we can derive the relation equation of voltages at LV and HV sides as

$$\frac{V_{Bat}}{V_{Bus}} = \frac{(1 - D_1)}{(1 + ND_1)} \tag{17}$$

From Equations (9) and (17) we can get that increasing the turns ratio can elevate the voltage conversion ratio; the relation between the turns ratio and voltage to be suffered while switch is off is expressed in the equation below [1]

$$v_{DS1} = V_{Bat} - v_{L1} = \frac{(V_{Bus} + NV_{Bat})}{(1 + N)} \tag{18}$$

$$v_{DS2} = v_{L2} + V_{Bus} = (V_{Bus} + NV_{Bat}) \tag{19}$$

Currents taken while all switches are on (closed) are expressed in Equations (20) and (21), where I_{Bus} is the DC link current, and I_B is the battery's current.

$$I_{DS1} = I_B + NI_{Bus} \tag{20}$$

$$I_{DS2} = \frac{I_B + NI_{Bus}}{(1 + N)} \tag{21}$$

To have the high voltage conversion ratio bidirectional converter operated at the continuous conduction mode (CCM), the design inductance must satisfy Equation (22) expressed below [1]

$$L_{1\min} = \frac{V_{Bat}R_{Bus}(V_{Bus} - V_{Bat})(1 - D_1)T}{2V_{Bus}^2(N + 1)} \tag{22}$$

where R_{Bus} is the load resistance at the high-voltage side of the DC voltage bus as shown in Figure 1.

3. **Controller Design of High Voltage Conversion Ratio Bidirectional Converter.** Figure 7 shows the system control frame of high voltage conversion ratio bidirectional converter; it contains two loop controllers: the inner loop is the battery current control loop; the outer loop is the DC link voltage control loop [19].

After going through the loop, the HV voltage V_{Bus} (i.e., DC link voltage) will generate a V'_{Bus} voltage signal, after compared with the referenced voltage V^*_{Bus}, it generates a voltage error signal ε_v; after being compensated by the voltage controller, it gets the commanding value of battery current i^*_o, after compared i^*_o with the battery feedback current i'_B, we obtain a current signal deviation signal ε_i; then, after being through the current controller, we obtain a tuning signal V_{cont}; then, after compared with the triangular carrier wave

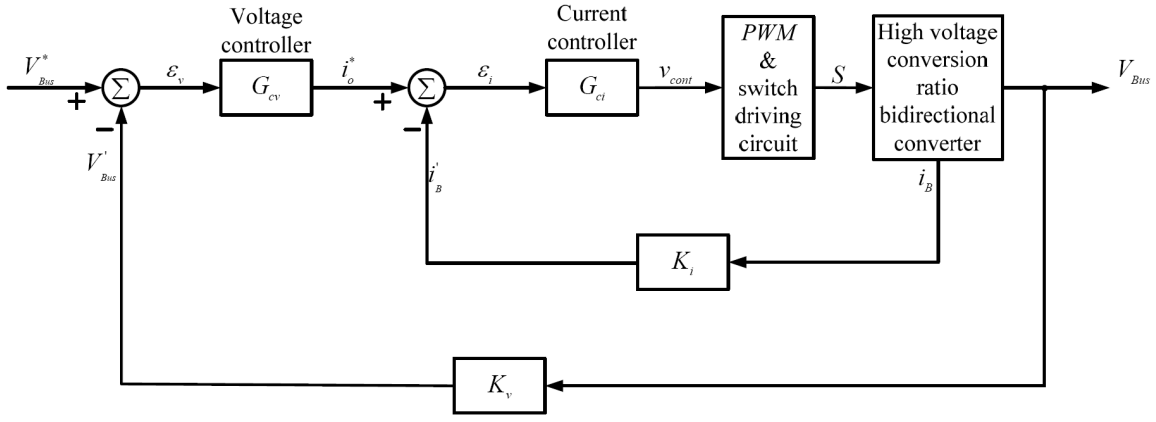

FIGURE 7. System control frame of high voltage conversion ratio bidirectional converter

signal, it generates the pulse width modulation (PWM) signal, used to control the switch state of power switches S_1 and S_2. If voltage deviation occurs at HV side, tuning the value and direction of battery current command i_o^* over the voltage control loop can ensure that the voltage at HV side is stabilized at the set command value.

3.1. **Design of current controller.** The current control of high voltage conversion ratio bidirectional converter is to have the high voltage conversion ratio bidirectional converter work at the continuous conduction mode (CCM) and make design [20,21]; in this paper, we let the converter work at boost mode and make analysis on it; treat both L_1 and L_2 as an equivalent inductor L. Since the controlled battery current is equal to the current at inductor L, while S_1 at LV is closed, its state equation can be expressed as

$$\begin{cases} \dfrac{di_B}{dt} = \dfrac{(1+N)v_{Bat}}{L} \\ \dfrac{dv_{C_H}}{dt} = -\dfrac{v_{Bus}}{R_{Bus}C_H}, \quad 0 \le t \le D_1T \\ v_{Bus} = v_{C_H}, \quad i_{S2} = 0 \end{cases} \tag{23}$$

After expressing Equation (23) in matrix, it becomes

$$\begin{cases} \dfrac{d}{dt}\begin{bmatrix} i_B \\ v_{C_H} \end{bmatrix} = \begin{bmatrix} 0 & 0 \\ 0 & -\dfrac{1}{R_{Bus}C_H} \end{bmatrix}\begin{bmatrix} i_B \\ v_{C_H} \end{bmatrix} + \begin{bmatrix} \dfrac{(1+N)}{L} \\ 0 \end{bmatrix} v_{Bat} \\ v_{Bus} = \begin{bmatrix} 0 & 1 \end{bmatrix}\begin{bmatrix} i_B \\ v_{C_H} \end{bmatrix}, \quad i_{S2} = 0 \end{cases} \tag{24}$$

While S_1 at LV is opened, its state equation can be expressed as

$$\begin{cases} \dfrac{di_B}{dt} = \dfrac{v_{Bat} - v_{Bus}}{L} \\ \dfrac{dv_{C_H}}{dt} = \dfrac{i_B}{C_H} - \dfrac{v_{Bus}}{R_{Bus}C_H}, \quad D_1T \le t \le T \\ v_{Bus} = v_{C_H}, \quad i_{S2} = i_B \end{cases} \tag{25}$$

After expressing Equation (25) in matrix, it becomes

$$\begin{cases} \dfrac{d}{dt}\begin{bmatrix} i_B \\ v_{C_H} \end{bmatrix} = \begin{bmatrix} 0 & -\dfrac{1}{L} \\ \dfrac{1}{C_H} & -\dfrac{1}{R_{Bus}C_H} \end{bmatrix}\begin{bmatrix} i_B \\ v_{C_H} \end{bmatrix} + \begin{bmatrix} \dfrac{1}{L} \\ 0 \end{bmatrix} v_{Bat} \\ v_{Bus} = \begin{bmatrix} 0 & 1 \end{bmatrix}\begin{bmatrix} i_B \\ v_{C_H} \end{bmatrix}, \quad i_{S2} = i_B \end{cases} \tag{26}$$

Next, we use the state average method [22-25] to average the state equation in S_1 switch's duty cycle, i.e., Equation (24) $\times D_1T$ + Equation (26) $\times (1-D_1)T$ and divided by T, we obtain

$$\begin{cases} \dfrac{d}{dt}\begin{bmatrix} i_B \\ v_{C_H} \end{bmatrix} = \begin{bmatrix} 0 & -\dfrac{(1-D_1)}{L} \\ \dfrac{(1-D_1)}{C_H} & -\dfrac{1}{R_{Bus}C_H} \end{bmatrix}\begin{bmatrix} i_B \\ v_{C_H} \end{bmatrix} + \begin{bmatrix} \dfrac{1+Nd_1}{L} \\ 0 \end{bmatrix} v_{Bat} \\ v_{Bus} = \begin{bmatrix} 0 & 1 \end{bmatrix}\begin{bmatrix} i_B \\ v_{C_H} \end{bmatrix}, \quad i_{S2} = (1-d_1)i_B \end{cases} \tag{27}$$

To linearize Equation (27), we add the disturbing signal at the operation point, i.e., $i_B = I_B + \Delta i_B$, $v_{C_H} = V_{C_H} + \Delta v_{C_H}$, $v_{Bat} = V_{Bat} + \Delta v_{Bat}$, $v_{Bus} = V_{Bus} + \Delta v_{Bus}$, $i_{S2} = I_{S2} + \Delta i_{S2}$ and $d_1 = D_1 + \Delta d_1$; after putting the disturbing signal into Equation (27), we get

$$\begin{cases} \dfrac{d}{dt}\begin{bmatrix} I_B + \Delta i_B \\ V_{C_H} + \Delta v_{C_H} \end{bmatrix} = \begin{bmatrix} 0 & -\dfrac{[1-(D_1+\Delta d_1)]}{L} \\ \dfrac{[1-(D_1+\Delta d_1)]}{C_H} & -\dfrac{1}{R_{Bus}C_H} \end{bmatrix} \begin{bmatrix} I_B + \Delta i_B \\ V_{C_H} + \Delta v_{C_H} \end{bmatrix} \\ \qquad\qquad + \begin{bmatrix} \dfrac{1+N(D_1+\Delta d_1)}{L} \\ 0 \end{bmatrix} V_{Bat} + \Delta v_{Bat} \\ V_{Bus} + \Delta v_{C_H} = \begin{bmatrix} 0 & 1 \end{bmatrix} \begin{bmatrix} I_B + \Delta i_B \\ V_{C_H} + \Delta v_{C_H} \end{bmatrix} \\ I_{S2} + \Delta i_{S2} = [1-(D_1+\Delta d_1)](I_B + \Delta i_B) \end{cases} \tag{28}$$

Set the disturbing value of Equation (28) to zero, we can get that the steady-state operation point is Equation (29), the disturbing signal equation at operation points (V_{Bat}, V_{Bus}, I_{S2}, I_L, D_1) is shown in Equation (30).

$$\begin{cases} V_{Bat} = V_{Bus}\dfrac{(1-D_1)}{1+ND_1} \\ V_{Bus} = V_{C_H} = (1-D_1)I_B R_{Bus} \\ I_{S2} = \dfrac{V_{Bus}}{R_{Bus}}, \quad I_{S2} = (1-D_1)I_B \end{cases} \tag{29}$$

$$\begin{cases} \dfrac{d\Delta i_B}{dt} = -\dfrac{(1-D_1)}{L}\Delta v_{C_H} + \dfrac{1+ND_1}{L}\Delta v_{Bat} + \dfrac{V_{C_H}+NV_{Bat}}{L}\Delta d_1 \\ \dfrac{d\Delta v_{C_H}}{dt} = \dfrac{(1-D_1)}{C_H}\Delta i_B - \dfrac{1}{R_{Bus}C_H}\Delta v_{C_H} - \dfrac{I_B}{C_H}\Delta d_1 \\ \Delta V_{Bus} = \Delta V_{C_H}, \quad \Delta i_{S2} = (1-D_1)\Delta i_B - I_B\Delta d_1 \end{cases} \tag{30}$$

After making Laplace transformation on Equation (30), we can plot the small signal dynamic model block diagram, shown in Figure 8. By doing so, it can control the loop current, where K_i is the current sensing factor.

After deriving, the transfer function $\left.\frac{\Delta i_B(s)}{\Delta d_1(s)}\right|_{\Delta v_{Bat}(s)=0}$ in Figure 8 can be the transfer function of Equation (31).

$$\left.\frac{\Delta i_B(s)}{\Delta d_1(s)}\right|_{\Delta v_{Bat}(s)=0} = \frac{(V_{Bus}+NV_{Bat})R_{Bus}C_H s + 2V_{Bus} + NV_{Bat}}{R_{Bus}C_H L s^2 + Ls + (1-D_1)^2 R_{Bus}} \tag{31}$$

The transfer function of current loop gain is

$$LG(s) = \frac{G_{ci}(s)\frac{1}{\hat{V}_{tri}}K_i\left[(V_{Bus}+NV_{Bat})R_{Bus}C_H s + 2V_{Bus} + NV_{Bat}\right]}{R_{Bus}C_H L s^2 + Ls + (1-D_1)^2 R_{Bus}} \tag{32}$$

where $\hat{V}_{tri}$ is the amplitude of triangular carrier wave. The current controller $G_{ci}(s)$ applies the PI controller shown in Equation (33).

$$G_{ci}(s) = \frac{K_{Pi}s + K_{Ii}}{s} \tag{33}$$

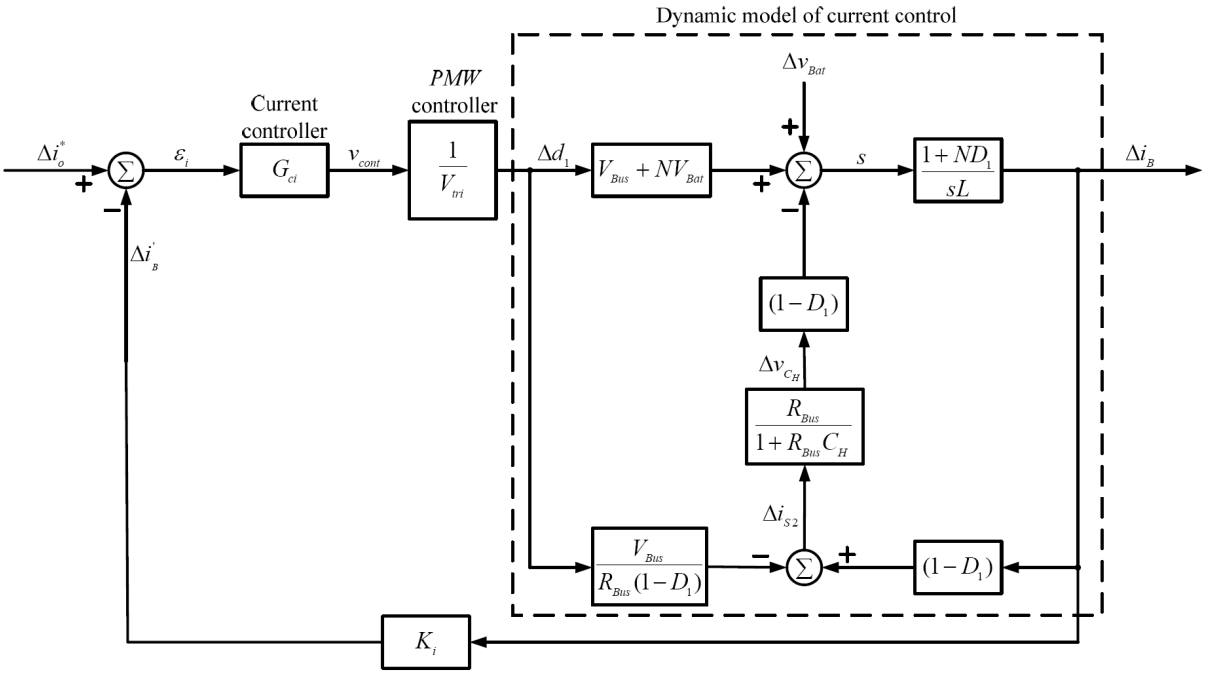

FIGURE 8. Control system block diagram of the input current of high voltage conversion ratio bidirectional converter

The derivation of dynamic model and controller quantitative design are pretty difficult, and we thus apply a simple general rule in the design process: the crossover frequency f_c is less than half of the switching frequency f_s [26], as expressed in Equation (34).

$$f_c < \frac{1}{2} f_s \tag{34}$$

Since the integration gain has less influence to the crossover frequency, we thus select $K_{Ii} = 10000$, and use the condition of Equation (33) to find out the range of K_{Pi}. Next, we use Matlab software to analyze the Bode plots for the different loop gain frequency responses corresponding to different K_{Pi} when $K_{Ii} = 10000$, shown in Figure 9. After the analysis, we get the condition of K_{Pi} as

$$|LG(s = j2\pi f_c)|_{\substack{K_{Ii} = 10000 \\ f_c = 25\text{kHz}}} = 1 \tag{35}$$

Here we set $K_{Pi} = 10$, and get the parameter of current feedback controller as

$$G_{ci}(s) = \frac{K_{Pi}s + K_{Ii}}{s} = \frac{10s + 10000}{s} \tag{36}$$

3.2. **Dynamic model estimation.** Next, we use the step-response method [27] to estimate the dynamic model of converter; the system dynamic response of high voltage conversion ratio bidirectional converter is expressed by the voltage loop control block diagram shown in Figure 10, where $K_v = 0.005$ is the voltage sensing factor due to a attenuation ratio 200:1 of the voltage sensor, K_{pv} is the conversion coefficient of the voltage change due to a power disturbance at HV side, $G_{cv}(s)$ is the voltage controller, and $G_p(s)$ is the transfer function of converter.

While estimating the dynamic mode by the step response estimation method, the design steps are as follows.

a) To estimate the dynamic mode estimation, the voltage controller was set as the proportional control $G_{cv}(s) = K_p = 3$ at the operation point ($V_{Bus} = 324$V, $P = 1000$W) to let the system operate in a closed loop control.
b) Given a step voltage command ($\Delta v^*_{Bus} = 0.2$, i.e., the voltage v_{Bus} at HV side changes 324V $\rightarrow$ 364V), the changing status of measured v_{Bus} is shown in Figure 11; the steady-state voltage is 360V.
c) At the same operating condition, grant an irradiance-change to make the change of module array output power become $\Delta P_{pv} = 150$W, i.e., P_{pv} changes 1000W $\rightarrow$ 850W, the response of measured v_{Bus} is shown in Figure 12; the steady-state voltage is 318V.

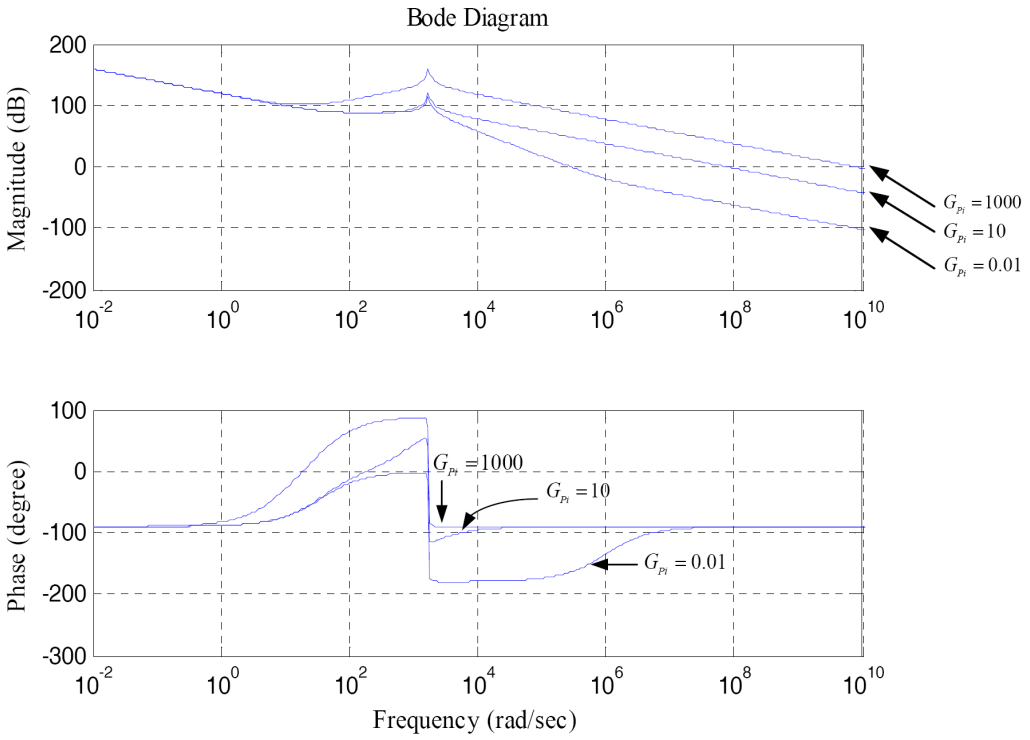

FIGURE 9. Bode plots for current loop frequency response

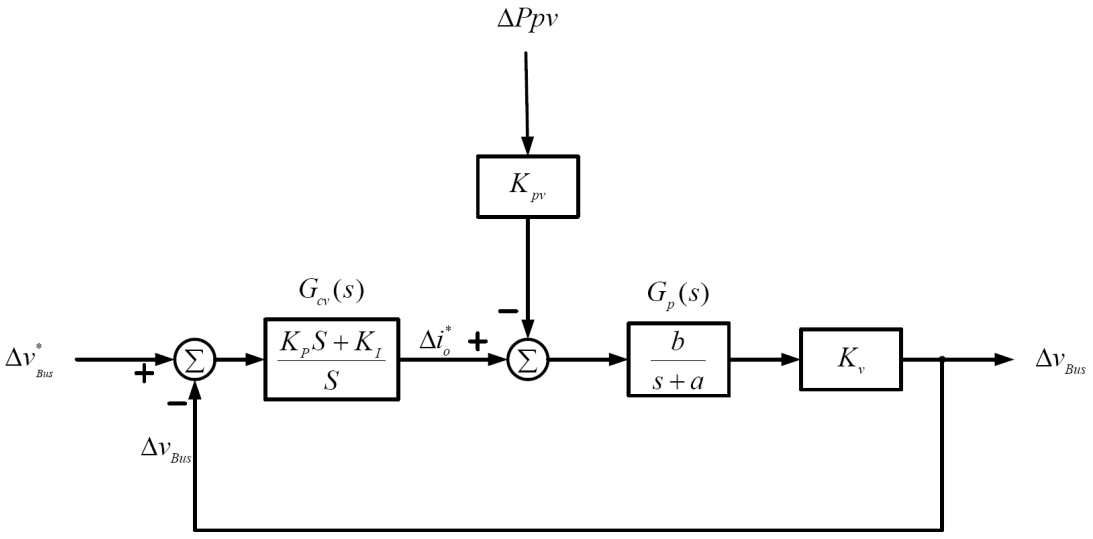

FIGURE 10. Voltage loop control block diagram for high voltage conversion ratio bidirectional converter

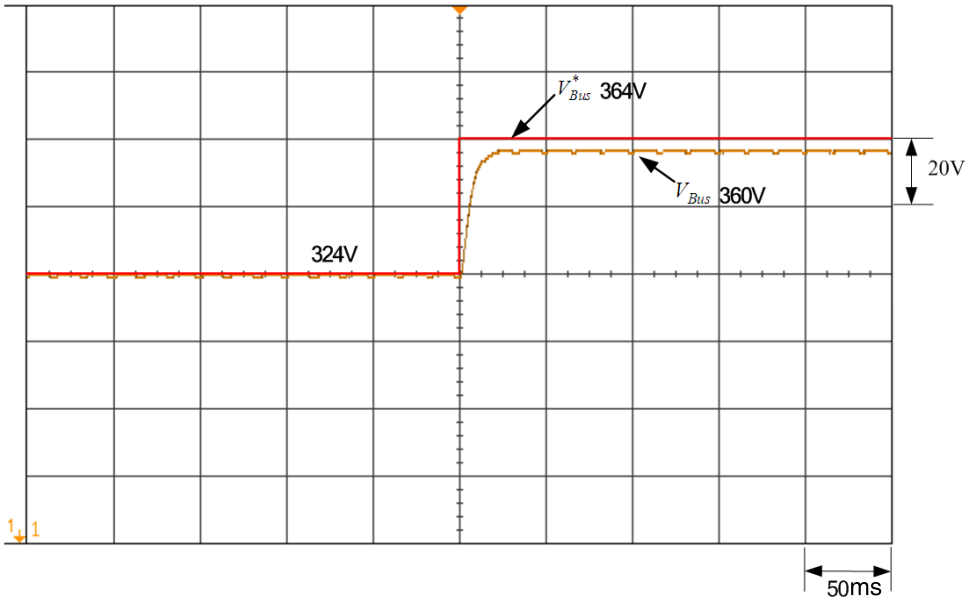

FIGURE 11. Output response waveform of DC link voltage step command for the change from 324V to 364V

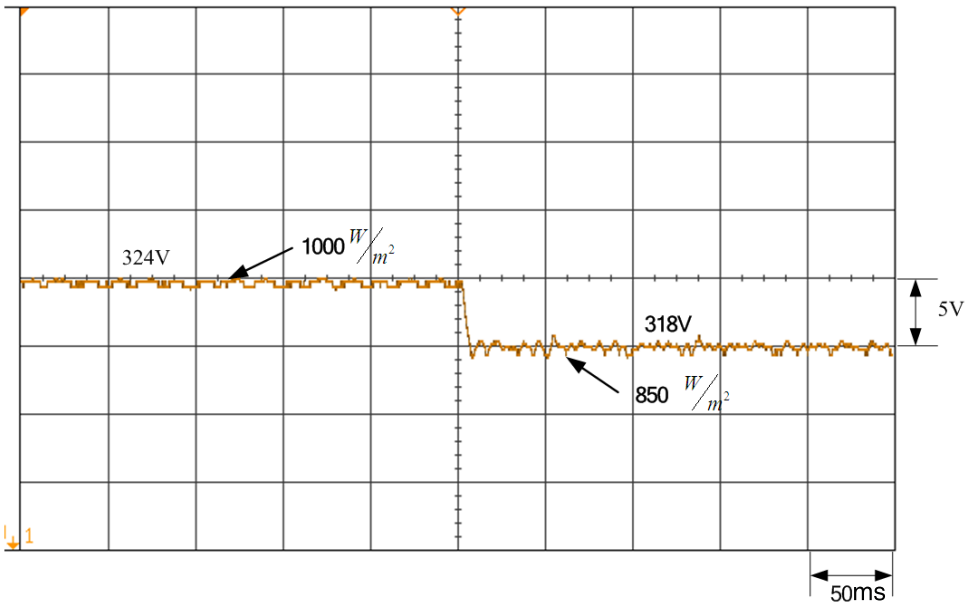

FIGURE 12. Output voltage waveform while irradiance changes from 1000W/m^2 down to 850W/m^2 (i.e., P_{pv} changes from 1000W $\rightarrow$ 850W)

d) From voltage control loop block diagram shown in Figure 10, we can derive the transfer functions of Equation (37) for Δv_{Bus} versus Δv^*_{Bus} and Equation (38) for Δv_{Bus} versus ΔP_{pv}.

$$H_v(s) = \left.\frac{\Delta v_{Bus}}{\Delta v^*_{Bus}}\right|_{\Delta p=0} = \frac{bG_{cv}K_v}{s+a+bG_{cv}K_v} \triangleq \frac{c_1}{s+d} \tag{37}$$

$$H_p(s) = \left.\frac{\Delta v_{Bus}}{\Delta P_{pv}}\right|_{\Delta v^*_{Bus}=0} = \frac{-bK_{pv}K_v}{s+a+bG_{cv}K_v} \triangleq -\frac{c_2}{s+d} \tag{38}$$

where

$$G_{cv} = K_p \tag{39}$$

$$d = a + bG_{cv}K_v = a + bK_pK_v \tag{40}$$

$$c_1 = bG_{cv}K_v = bK_pK_v \tag{41}$$

$$c_2 = bK_{pv}K_v \tag{42}$$

e) We can get the time of obtaining the steady-state value of voltage step-response and time of reaching $(1 - e^{-1})$ of steady-state value from Figure 11, and calculate the parameters $c_1 = 145.775$ and $d = 166.6$.

f) From Figure 12 we can see the steady-state response of step change for irradiance (i.e., $\Delta p_{pv} = 150$W), from Equation (38) we can calculate $c_2 = 0.033$, and from Equations (41) and (42) we get $K_{pv} = 0.0006857$.

g) From Equations (39) to (42) we can get $a = 20.8255$ and $b = 9718.3$, the transfer function of converter $G_p(s)$ is shown in Equation (43).

$$G_p(s) = \frac{b}{s+a} = \frac{9718.3}{s+20.8255} \tag{43}$$

3.3. **Design of voltage controller.** In the control block diagram of Figure 10, we set $\overline{a} = 20.8255$ and $\overline{b} = K_v b = 0.005 \times 9718.3 = 48.5915$ to express the estimated dynamic model parameter of converter, and DC link voltage controller $G_{cv}(s)$ applies the PI controller displayed in Equation (44).

$$G_{cv}(s) = \frac{K_P s + K_I}{s} \tag{44}$$

From the control block diagram shown in Figure 10, we can derive the closed loop transfer function from Δv_{Bus} to ΔP_{pv} as shown in Equation (45).

$$H_P(s) = \left.\frac{\Delta v_{Bus}}{\Delta P_{pv}}\right|_{\Delta v^*_{Bus}=0} = \frac{-sK_{pv}\overline{b}}{s^2 + \left(\overline{a} + \overline{b}K_P\right)s + \overline{b}K_I} \tag{45}$$

The unit-step response of (45) is

$$\Delta v_{Bus}(s) = \frac{H_P(s)}{s} = \frac{-K_{pv}\overline{b}\Delta p}{s^2 + \left(\overline{a} + \overline{b}K_P\right)s + \overline{b}K_I} \tag{46}$$

To have system get the high-performance regulation characteristics, normally the step dynamic response should have zero steady-state error, zero overshoot, small maximum-voltage-dip and short restore time. To have the aforesaid characteristics, define the restore time t_r is the time of voltage restoring back to 5% of maximum voltage-dip after the irradiance changes. After deciding the standards of maximum voltage-dip $\hat{v}_{Bus,\max}$ and restoring time t_r, we can obtain the following two nonlinear equations.

$$f_1(u_1, u_2) = \hat{v}_{Bus,\max} - \frac{K_{pv}\overline{b}\Delta P_{pv}}{u_1 - u_2}\left[e^{\frac{-u_1}{u_1-u_2}\ln\left(\frac{u_1}{u_2}\right)} - e^{\frac{-u_2}{u_1-u_2}\ln\left(\frac{u_1}{u_2}\right)}\right] \tag{47}$$

$$f_2(u_1, u_2) = 0.05\hat{v}_{Bus,\max} - \frac{K_{pv}\overline{b}\Delta P_{pv}}{u_1 - u_2}\left[e^{-u_1 t_r} + e^{-u_2 t_r}\right] \tag{48}$$

$$\begin{aligned} u_1 + u_2 &= \overline{a} + \overline{b}K_P \\ u_1 u_2 &= \overline{b}K_I \end{aligned} \tag{49}$$

In Figure 10 (voltage feedback control block diagram), since the controller has integrator, system thus has no steady-state error. When Equation (45) solves out that both the two characteristic roots are the negative real numbers, it thus can prove that no overshoot exists [28], which can satisfy the conditions of Equations (47) and (48). After t_r and $\hat{v}_{Bus,\max}$ are given, we can use Matlab software to solve the variables u_1 and u_2 ($u_1 > 0$,

$u_2 > 0$) of equations $f_1(u_1, u_2)$ and $f_2(u_1, u_2)$; then, we use Equation (49) to solve the parameters K_P and K_I of DC link voltage controller:

$$K_P = \frac{(u_1 + u_2) - \overline{a}}{\overline{b}} \qquad K_I = \frac{u_1 u_2}{\overline{b}} \tag{50}$$

4. **Simulation and Experimental Results.** Table 1 lists the electrical specifications and component ratings of the implemented high voltage conversion ratio bidirectional converter. This paper mainly focuses on the design of controller of the proposed converter. As for the design procedure of the converter's circuit element specification, the previous paper has already presented in [2]; therefore, in view of the limited length of the paper, it does not repeat here. The dynamic model of this converter is derived as shown in Equation (51); we make test on the controller we have designed at the specified operating point (output voltage $v_{Bus} = 324$V and load power $P_{pv} = 1000$W).

$$G_p(s) = \frac{\overline{b}}{s + \overline{a}} = \frac{48.6}{s + 20.8255} \tag{51}$$

TABLE 1. Electrical specifications and component ratings involved in the implemented converter

Parameter	Specification
Low voltage side voltage (V_{Bat})	$V_{Bat} = 50$V
High voltage side voltage (V_{Bus})	$V_{Bus} = 380$V
Switching frequency (f)	$f = 25$kHz
Power rating (P_o)	$P_o = 1000$W
Coupled inductance (L_1, L_2)	$L_1 = 20\mu$H, $L_2 = 80\mu$H
Turn ratio of coupled inductor (N)	$N = 2$
Power switches (S_1, S_2)	IXGH48N60C3D1 (600V/48A)
Capacitance (C_L, C_H)	$C_L = C_H = 470\mu$F

The controller performances to be met are:

a) Steady-state error = 0;
b) Overshoot = 0;
c) Maximum output voltage-dip made from the change of step irradiance $\hat{v}_{Bus,\max} = 0.1$V/W (i.e., 150W $\rightarrow$ 15V);
d) Restoring time caused by the change of step irradiance $t_r = 0.1$ sec.

Applying the quantitative controller design method of controller, we can get the voltage controller parameter of DC link from Equation (50):

$$K_P = 0.085, \quad K_I = 2.519 \tag{52}$$

In order to verify the feasibility of quantitative design on controller, under the step-change of 150W module array output power, the simulated DC link step-response is shown in Figure 13.

The simulating result shows that the output's voltage dynamic response meets the set condition (maximum voltage-dip is 15V, and the restoring time is 0.1sec). At the same condition, Figures 14 and 15 show the DC link voltage dynamic response measured by applying the controller under quantitative design ($K_P = 0.085$, $K_I = 2.519$) and traditional PI controller ($K_P = 0.05$, $K_I = 3$) respectively. From Figure 14 we can see that for the controller that applies quantitative design, the output voltage dynamic response meets the results made by simulation. And from Figure 15 we can see that for

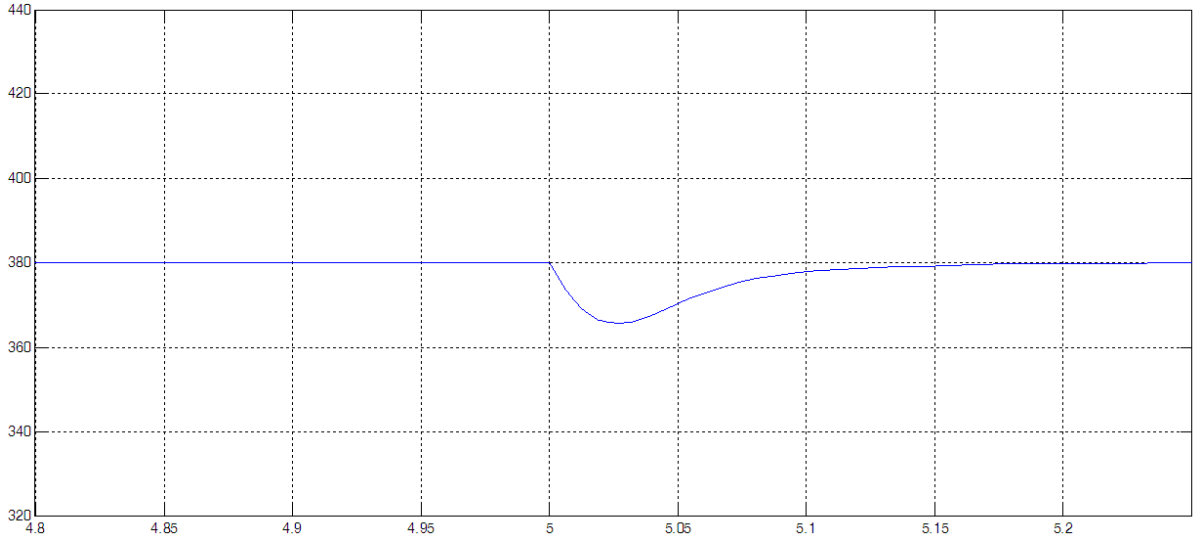

FIGURE 13. Simulated output DC link voltage waveform of photovoltaic module array made by applying the quantitatively designed controller under Δ150W (1000W $\rightarrow$ 850W) power change

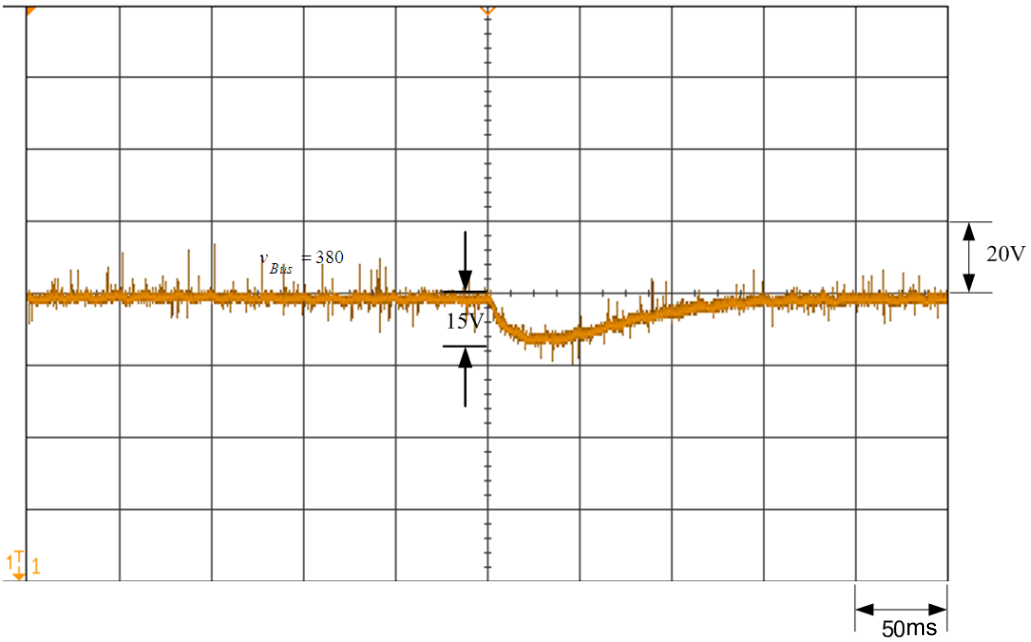

FIGURE 14. Measured output DC link voltage waveform of photovoltaic module array made by applying the quantitatively designed controller under Δ150W (1000W $\rightarrow$ 850W) power change

the traditional PI controller, although the voltage-dip has insignificant difference from the one shown in Figure 14, the restoring time takes longer apparently.

While the photovoltaic module array power output is down for 250W, the measured dynamic response of output voltage is shown in Figure 16. Although the 250W power step change is in excess of the designed one, which makes the voltage-dip a little bit higher, it is still better than the control performance of traditional PI controller shown in Figure 17, in particular on the brilliance of restoring time.

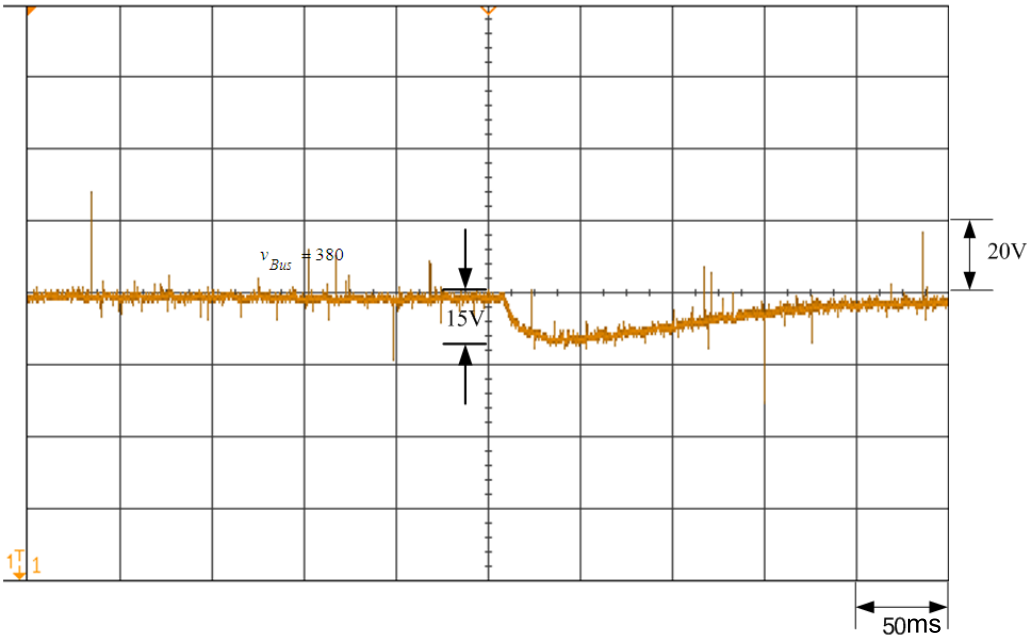

FIGURE 15. Measured output DC link voltage waveform of photovoltaic module array made by applying the traditional PI controller under Δ150W power change

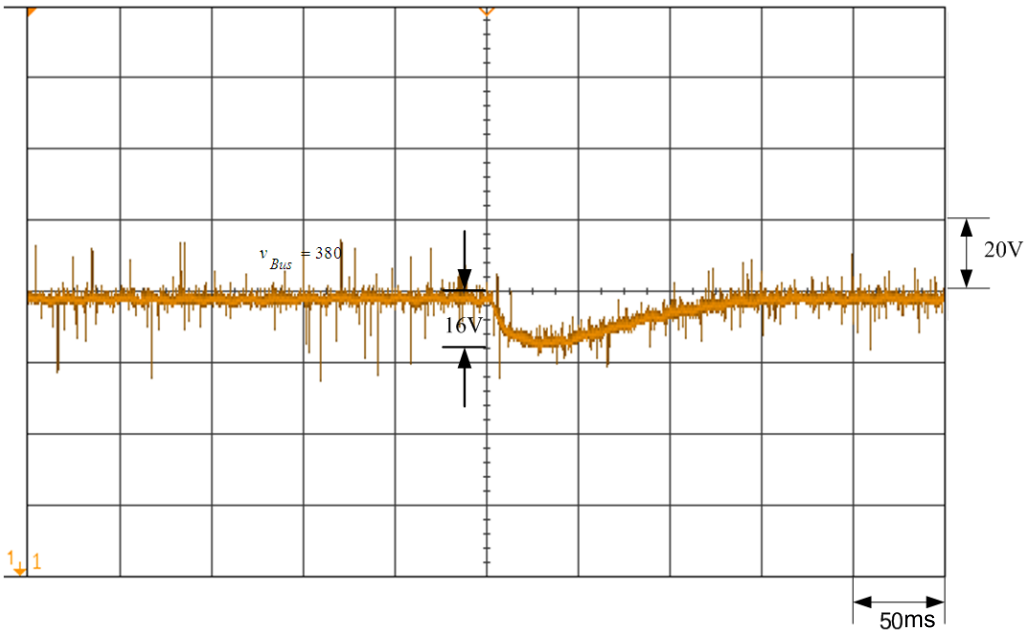

FIGURE 16. Measured output DC link voltage waveform of photovoltaic module array made by applying the quantitatively designed controller under Δ250W (1000W $\rightarrow$ 750W) power change

5. **Conclusions.** In this paper we build a high voltage conversion ratio bidirectional converter, which can sustain a stable DC link voltage output when the photovoltaic module array output power varies, and supplies sufficient power to load while the irradiance is insufficient; while the irradiance is sufficient, it can store the extra power into battery. Meanwhile, the voltage controller applying quantitative design enables DC link voltage to have high regulation performance. The high voltage-ratio bidirectional converter made in

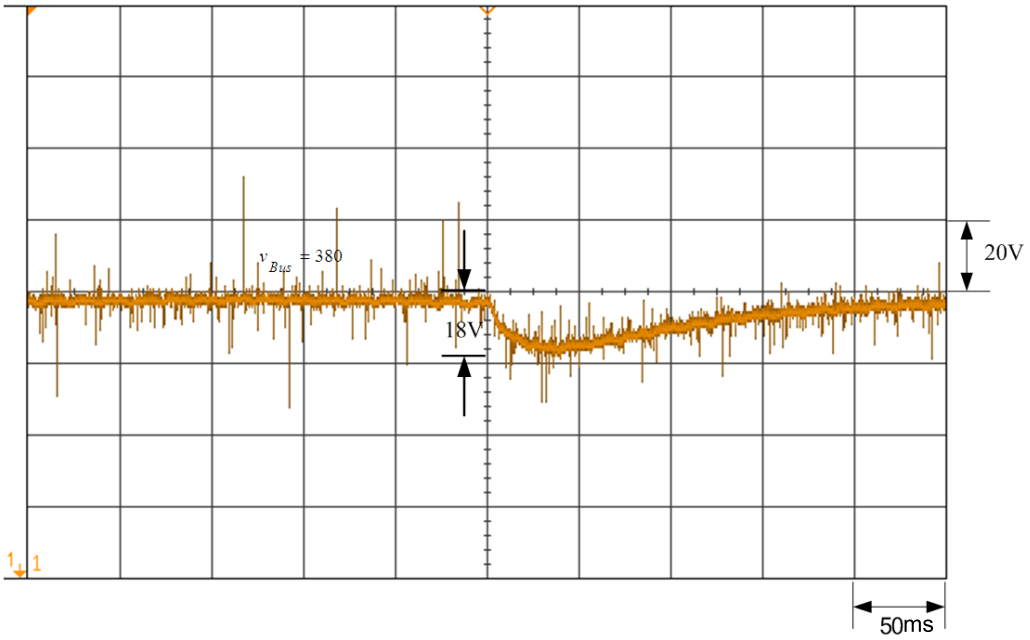

FIGURE 17. Measured output DC link voltage waveform of photovoltaic module array made by applying the traditional PI controller under Δ250W power change

this paper also can be applied in different renewable energies; the applications are wide with practical value. A non-isolated soft-switching bidirectional converter will be studied in the future to provide not only a high conversion ratio, but also a low voltage stress across power switches. Furthermore, the surge voltage can be suppressed through the release of the energy stored in leakage inductance. In addition, a robust PI voltage controller with a quantitative design procedure will be presented to overcome a wide range of load changes.

REFERENCES

[1] Y. M. Chen, H. C. Wu and Y. C. Chen, DC bus regulation strategy for grid-connected PV power generation system, *Proc. of IEEE International Conference on Sustainable Energy Technologies (ICSET)*, pp.437-442, 2008.

[2] B. L. Narasimharaju, S. P. Dudey and S. P. Singh, Coupled inductor bidirectional DC-DC converter for improved performance, *Proc. of IEEE International Conference on Industrial Electronics Control and Robotics (IECR)*, pp.28-33, 2010.

[3] B. L. Narasimharaju, S. P. Dudey and S. P. Singh, A novel voltage clamped CI-BDC converter and its control for battery storage applications, *Proc. of IEEE International Conference on Power Electronics, Drives and Energy Systems (PEDES)*, 2010.

[4] P. Tyagi, V. C. Kotak and V. P. S. Singh, Design high gain DC-DC boost converter with coupling inductor and simulation in PSIM, *International Journal of Research in Engineering and Technology (IJRET)*, vol.3, pp.156-163, 2014.

[5] J. C. Lopez, M. Ortega and F. Jurado, New topology for DC-DC bidirectional converter for hybrid systems in renewable energy, *International Journal of Electronics*, vol.102, pp.418-432, 2015.

[6] J. C. S. Júniora, J. P. R. Balestero and F. L. Tofoli, Novel bidirectional DC-DC converters based on the three-state switching cell, *International Journal of Electronics*, vol.103, pp.878-897, 2015.

[7] B. L. Narasimharaju, S. P. Dudey and S. P. Singh, Voltage mode control of coupled inductor bidirectional DC to DC converter, *Proc. of IEEE International Conference of Electron Devices and Solid-State Circuits (EDSSC)*, pp.1-6, 2010.

[8] B. L. Narasimharaju, S. P. Dudey and S. P. Singh, Parasitic effect considerations in modeling of CI-BDC converter and its voltage controller, *Proc. of International Conference on Power Electronics, Drives and Energy Systems (PEDES)*, 2010.
[9] A. U. S. Jyothi, D. S. P. Gopal and G. Ramu, Bi-directional DC-DC converter drive with PI and fuzzy logic controller, *International Journal of Advanced Research in Electrical, Electronics and Instrumentation Engineering (IJAREEIE)*, vol.2, pp.5435-5441, 2013.
[10] N. F. N. Ismail, I. Musirin, R. Baharom and D. Johari, Fuzzy logic controller on DC/DC boost converter, *Proc. of IEEE International Conference on Power and Energy (PECON)*, pp.661-666, 2010.
[11] A. Romero, L. Martinez-Salamero, H. Valderrama, O. Pallas and E. Alarcon, General purpose sliding-mode controller for bidirectional switching converters, *Proc. of IEEE International Symposium on Circuits and Systems*, pp.466-469, 1998.
[12] D. S. Oh, Y. J. Kim, J. D. La and Y. S. Kim, The sliding mode controller of the bidirectional converter for the DC bus stabilization, *Proc. of International Conference on Electrical Machines and Systems (ICEMS)*, pp.367-371, 2010.
[13] A. T. Laura, V. I. Enric, M. A. Javier, M. P. Sylvia and M. S. Luis, Seamless sliding-mode control for bidirectional boost converter with output filter for electric vehicles applications, *IET Power Electronics*, vol.8, pp.1808-1816, 2015.
[14] P. Akter, M. Uddin, S. Mekhilef, N. M. L. Tan and H. Akagi, Model predictive control of bidirectional isolated DC-DC converter for energy conversion system, *International Journal of Electronics*, vol.102, pp.1407-1427, 2015.
[15] M. Takahashi, Self-repairing PI/PID control against sensor failures, *International Journal of Innovative Computing, Information and Control*, vol.12, no.1, pp.193-202, 2016.
[16] S. Gao, X. Wu, G. Wang and G. Zhang, The immune fuzzy PID stripper temperature control algorithm based on chaotic optimization, *International Journal of Innovative Computing, Information and Control*, vol.12, no.1, pp.103-112, 2016.
[17] F. Liu and H. Wang, Fuzzy PID tracking controller for two-axis airborne optoelectronic stabilized platform, *International Journal of Innovative Computing, Information and Control*, vol.13, no.4, pp.1307-1322, 2017.
[18] R. Kurokawa, N. Inoue, T. Sato, O. Arrieta, R. Vilanova and Y. Konishi, Simple optimal PID tuning method based on assigned robust stability -Trade-off design based on servo/regulation performance-, *International Journal of Innovative Computing, Information and Control*, vol.13, no.6, pp.1953-1963, 2017.
[19] D. Buvana and R. Jayashree, Current control in two level non-isolated bidirectional DC-DC converter in CCM for HEV, *Proc. of IET Chennai 4th International Conference on Sustainable Energy and Intelligent Systems (SEISCON)*, pp.228-239, 2013.
[20] D. W. Hart, *Introduction to Power Electronics*, Pearson Education, New York, 1997.
[21] F. H. Zhang, C. H. Zhu and Y. G. Yan, The controlled model of bi-directional DC-DC converter, *Proc. of the Chinese Society for Electrical Engineering (CSEE)*, vol.25, pp.46-79, 2005.
[22] R. D. Middlebrook and S. Cuk, A general unified approach to modeling switching converter power stages, *Proc. of IEEE Power Electronics Specialists Conference*, pp.18-34, 1976.
[23] R. D. Middlebrook, S. Cuk and W. Behen, A new battery charger/discharger converter, *Proc. of IEEE Power Electronics Specialists Conference*, pp.251-255, 1978.
[24] S. P. Hsu, A. Brown, L. Rensink and R. D. Middlebrook, Modelling and analysis of switching DC-to-DC converters in constant-frequency current-programmed mode, *Proc. of IEEE*, 1979.
[25] C. K. Tse and K. M. Adams, Quasi-linear modeling and control of DC-DC converters, *IEEE Trans. Power Electronics*, vol.7, pp.315-323, 2002.
[26] R. Paul, L. Sankey, L. Corradini, Z. Popovic and D. Maksimovic, Power management of wideband code division multiple access RF power amplifiers with antenna mismatch, *IEEE Trans. Power Electronics*, vol.25, pp.981-991, 2009.
[27] K. H. Ang, G. Chong and Y. Li, PID control system analysis, design, and technology, *IEEE Trans. Control Systems Technology*, vol.13, pp.559-576, 2005.
[28] C. M. Liaw, Design of a two-degree-of-freedom controller for motor drives, *IEEE Trans. Automatic Control*, vol.37, pp.1215-1220, 1992.